NANO LETTERS

pubs.acs.org/NanoLett

Oxygen-Assisted Unidirectional Growth of CdSe Nanorods Using a Low-Temperature Redox Process

Jonathan D. Doll,[†] Ghanshyam Pilania,[§] Ramamurthy Ramprasad,[§] and Fotios Papadimitrakopoulos*[,†,‡]

[†]Nanomaterials Optoelectronics Laboratory (NOEL), Polymer Program, [‡]Department of Chemistry, [§]Department of Chemical, Materials and Biomolecular Engineering, and Institute of Materials Science, University of Connecticut, Storrs, Connecticut 06269-3136

ABSTRACT The role of oxygen in directing the low temperature (125 °C), redox-assisted, unidimensional *and* unidirectional growth of CdSe nanocrystals (NCs) was investigated. In the presence of oxygen, CdSe quantum dots grow selectively along their *c* axis with little to no change in their width. Reduction of oxygen in the growth medium results in three-dimensional growth. Moreover the one-dimensional growth was found to occur only from one of the two inequivalent polar (0001) facets, as supported by the seeded growth of $Cd_xHg_{1-x}Se$ onto CdSe seeds. This is in agreement with density functional theory simulations, which indicate that due to selective oxygen passivation growth can occur only along the [0001] direction. The ability to control seeded NC growth with respect to morphology and directionality opens new possibilities toward the low temperature synthesis of complex nanostructures.

KEYWORDS Nanocrystal, nanorod, seeded unidirectional growth

One-dimensional (1D) nanocrystals (NCs), known as quantum rods (QRs), possess unique optical properties such as linearly polarized emission and higher Stokes shift when compared to zero-dimensional NCs such as quantum dots (QDs).[1,2] From a device standpoint, the larger aspect ratio of QRs along with the ability to engineer heterojunctions, render them more advantageous than QDs.[3−7] Typically, solution-based synthesis of QRs involves the use of high-temperature media (i.e., 150−300 °C) and surfactants with appropriate structure and functionality to direct the 1D growth from either homogeneous growth,[1,2,8,9] or QD seeds.[4,5] Partial or complete removal of surfactants can lead to either excessive 3D growth and precipitation[10] or, under certain conditions, QD oriented attachment and fusion.[11] Our group has recently introduced a low temperature (125 °C) redox-based synthesis of QRs from QD seeds,[12] where a small molecular weight compound (i.e., aminopropanol (APOL)) is used as both solvent and coordinating ligand. In this contribution we show that by changing the oxygen concentration of the growth medium, the growth can be directed from 3D to 1D. Moreover, 1D growth was found to occur along the *c* axis, and more specifically on the (0001) facet as opposed to the (000$\bar{1}$) facet. This is supported by density functional theory (DFT) simulations which indicate that oxygen provides adequate passivation on all but the (0001) facet.

Our previous studies on the redox chemistry of CdSe NCs have shown that dissolved oxygen in a 9:1 APOL:H_2O (9:1 v/v) mixture is key for both faceted-etching at 85 °C[13,14] and QD-seeded growth to yield QRs at 125 °C.[12] Both processes are spontaneously initiated by the surface oxidation of CdSe according to eq 1.[13−20]

$$CdSe + {}^{3}/_{2}O_2 \rightarrow CdSeO_3 \quad (1)$$

Subsequent oxide dissolution can occur according to eq 2−4, depending on the facet-nature of the oxide

$$SeO_2 + H_2O \rightleftharpoons H_2SeO_3 \quad (2)$$

$$H_2SeO_3 + 2HO(CH_2)_3NH_2 \rightleftharpoons [HO(CH_2)_3NH_3^+]_2SeO_3^{2-} \quad (3)$$

$$CdO + 2HO(CH_2)_3NH_2 + [HO(CH_2)_3NH_3^+]_2SeO_3^{2-} \rightleftharpoons [Cd[HO(CH_2)_3NH_2]_4]^{2+}SeO_3^{2-} + H_2O \quad (4)$$

Equation 2 converts the Se-rich facets (i.e., SeO_2) to H_2SeO_3, a reaction that quickly occurs in the presence of water. Because APOL is basic, the neutralization of H_2SeO_3 sites to form a salt (eq 3) occurs rapidly and leads to the dissolution of the oxidized Se sites. Dissolution of the oxidized Cd sites

* Correspondence e-mail, papadim@mail.ims.uconn.edu.
Received for review: 11/16/2009
Published on Web: 01/22/2010

© 2010 American Chemical Society

DOI: 10.1021/nl903843g | *Nano Lett.* **2010,** *10,* 680-685

takes place through complexation with APOL (eq 4) and can be slowed by providing of excess Cd^{2+} ions through the addition of $CdCl_2$.[13] At 85 °C, and in the presence of $CdCl_2$, eqs 1−4 result in the formation of Cd-rich faceted CdSe NCs.[13]

When the temperature of the media is increased from 85 to 125 °C, a new reaction takes place (eq 5) in which H_2SeO_3 is reduced to Se^0.[21] Under the basic APOL conditions, and in the presence of H_2O, Se^0 disproportionates to Se^{2-} and SeO_3^{2-} (eq 6).[21] This provides the Se^{2-} source that, together with the added Cd^{2+} ions, facilitates further CdSe growth.[12]

$$H_2SeO_3 \rightleftharpoons Se^0 + H_2O + O_2 \quad (5)$$

$$3Se^0 + 3H_2O \rightleftharpoons 2Se^{2-} + SeO_3^{2-} + 6H^+ \quad (6)$$

In our previous communications, we suggested that oxygen may have a role in directing the growth of CdSe NCs to QRs.[12,20] In this contribution, we systematically investigate the role of oxygen, in conjunction with DFT calculations, on the relative stability of the oxide on the various facets. Studies of bulk CdSe have shown that oxygen tends to adsorb more strongly to the stoichiometric $(11\bar{2}0)$ facets (containing both Cd and Se atoms at equimolar amounts) to form $CdSeO_3$ as opposed to the polar (0001) and $(000\bar{1})$ facets, which are terminated by either Cd or Se atoms.[19] Since the $(10\bar{1}0)$ and $(01\bar{1}0)$ facets of wurtzite CdSe are also stoichiometrically populated with Cd and Se atoms, these might experience similar passivation to that of the $(11\bar{2}0)$ facet. These three facets are the most common QR sidewall facets, the passivation of which could explain the observed 1D growth.[20,23,24] With this in mind, two possible situations, outlined in Figure 1a, can arise under oxygenated conditions: Case A describes a situation where the energies of the polar (0001) and $(000\bar{1})$ facets are equivalent after oxygen passivation and both grow equally. Case B describes a situation where the energies of the (0001) and $(000\bar{1})$ facets differ, resulting in different growth rates. If indeed oxygen passivates more strongly the stoichiometric facets, its removal should result in incomplete passivation and promote three-dimensional growth (case C).

To test this, solutions of CdSe in APOL were made under differing oxygen conditions. A typical growth solution consists of CdSe QDs dissolved in a 9:1 APOL:H_2O mixture with an optical density (OD) of 4.0 at the first absorption maximum. Excess $CdCl_2$ was added to slow the NC etching as outlined above (eq 4) and to provide a Cd^{2+} source for growth. The Se^{2-} source originates from the slow etching of the smaller sized QDs in the starting suspension in accordance with eqs 5 and 6. More detailed experimental procedures and conditions can be found in the Supporting Information.

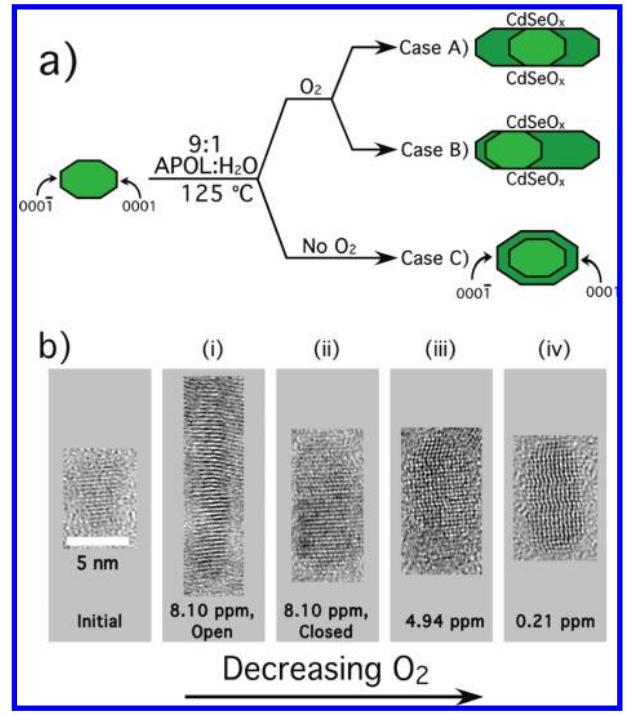

FIGURE 1. (a) Scheme showing NC growth in the presence and absence of oxygen. In the presence of oxygen, CdSe grows along the 0001 axis due to sidewall $CdSeO_x$ passivation. Cases A and B indicate two possible scenarios based on equal or unequal reactivity of the (0001) and $(000\bar{1})$ polar facets. In the absence of O_2, three-dimensional growth takes place due to incomplete oxide passivation. (b) HRTEM images of representative CdSe NCs after growth at 135 °C for various oxygen concentrations. The 5 nm scale bar applies to all of the images.

Four different growth conditions were investigated: sample i was left open to atmospheric conditions for the duration of the growth period, resulting in an equilibrium O_2 concentration of ca. 8.1 ppm; sample ii was sealed in glass under atmospheric conditions (i.e., the initial O_2 concentration was 8.1 ppm and as the reaction progresses it gradually decreases), and samples iii and iv had three and five freeze−pump−thaw (FPT) cycles performed on them, resulting in initial O_2 concentrations of 4.9 and 0.2 ppm, respectively. Following sample preparation, samples i−iv were annealed at 125 °C for 4 days. Subsequently, APOL was removed and replaced with a 10/20/70 wt % mixture of TOPO/TOP/*n*-octylamine to suppress further etching and render them soluble in chloroform.

Figure 1b shows representative HRTEM images of the CdSe NCs in the starting (seed) and the four grown NC samples. When compared to the starting CdSe seeds, the nanocrystals in sample i, where oxygen is abundant, have grown significantly along their *c* axis, although their width does not change appreciably. On the other hand, the O_2-restricted samples show a progressive increase in their width as the starting O_2 concentration decreases (TEM images showing a larger number of NCs in each of the samples can be found in Figures S1−S5 in the Supporting Information).

© 2010 American Chemical Society

DOI: 10.1021/nl903843g | *Nano Lett.* **2010,** *10,* 680-685

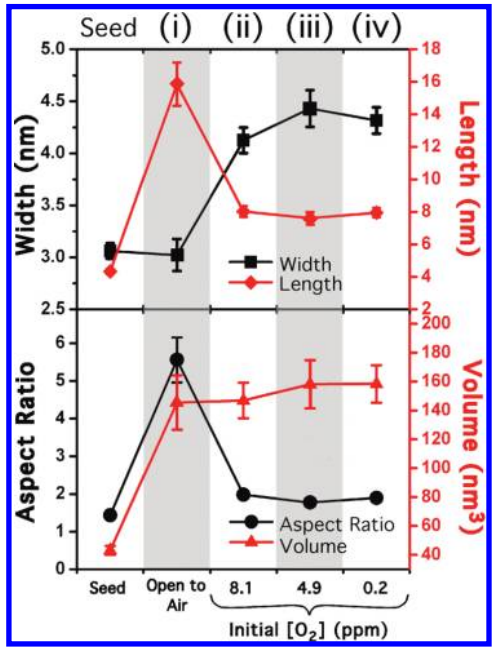

FIGURE 2. Length, width aspect ratio, and volume dependence of initial CdSe seed and after 4 days of growth at 125 °C under different oxygen concentrations.

To obtain a better picture of the role of oxygen on the average length, width, aspect ratio (length/width) and volume (length × width^2) of the NCs, a large number (ca. 100−150) of them were investigated by HRTEM and plotted in Figure 2, along with error bars reflecting their 95% confidence levels (actual histograms are shown in Figures S1−S5 in the Supporting Information). When oxygen is abundant (sample i), the NCs nearly quadruple their length along the 0001 direction but exhibit little change in their average width, indicative of 1D growth. Oxygen-restricted samples grow more three-dimensionally, showing significantly less elongation along the 0001 axis, while increasing in diameter. This effect is better seen in the plot of the average aspect ratio which displays a jump from 1.5 to 5.5 for sample i, while samples ii−iv exhibit a more modest increase to (ca. 2.0). What is more important, however, is that the average volume of all the grown NCs remains the same regardless of oxygen concentration. This signifies that all NCs experience the same growth kinetics, which appears to be controlled by the generation of the reaction-limiting Se^{2-} reagent due to the gradual etching of the smaller CdSe QDs in the growth solution. Here, it is important to stress that the generation of Se^{2-} is independent of O_2 concentration since the consumed oxygen in eq 1 is regenerated from eq 5, and oxygen only affects the surface passivation. The constant volume growth of NCs in samples i through iv also rules out any possibility for an oriented attachment mechanism.[11]

Barnard et al.[23] has simulated the low temperature growth of CdSe nanowires as a function of amine coverage and found that the differential facet binding can lead to aspect ratios ranging from 2.0 to 3.5. Furthermore, they concluded that in order to obtain higher aspect ratios, the need of an "external agent" must be added to arrest the sidewall growth of the rod.[23] From the 5.5 aspect ratio of sample i, it appears that oxygen acts as the referred "external agent."

Recent computational studies by Pilania, et al., have shown that under Cd-rich conditions, oxygen causes reduction in the surface energy of the nonpolar facets of wurtzite CdSe, while the surface energy of the polar facets remains relatively unchanged.[20] As an extension to this study, and in order to obtain a more complete understanding of the role of oxygen in surface passivation, a DFT study was performed to investigate the surface energy of the nonpolar $(10\bar{1}0)$, $(01\bar{1}0)$, and $(11\bar{2}0)$ facets along with the polar (0001) and $(000\bar{1})$ facets with 100% and 0% oxygen passivation. The polar facets are not equivalent, and the Cd- versus Se-terminated (0001) facets contain surface atoms with one and three dangling bonds, respectively. Similarly, the Cd- and Se-terminated $(000\bar{1})$ facets are decorated with surface atoms that display three and one dangling bonds, respectively. For the polar facets, the four different configurations shown in Figure 3 illustrate the (0001)Cd, (0001)Se, $(000\bar{1})$Cd, and $(000\bar{1})$Se surface configurations. Here, the element following the facet-bracket indicates the terminating surface atom. Parts a and b of Figure 3 illustrate the surface configuration prior to and after energy minimization, with the latter relaxed until the forces on each atom were <0.04 eV/Å. More details of these simulations are given in the Materials and Methods section of the Supporting Information.

In the wurtzite CdSe structure a Cd atom shares its two 5s electrons with six $4s^24p^4$ electrons of a Se atom to make four Cd to Se bonds. This leads to an electron donation pattern of 1/2 and 3/2, for Cd and Se, respectively, in the bulk environment. When the surface facets are allowed to relax, the system lowers its energy by redistributing the electrons of the surface dangling bonds. In the case of the nonpolar facets, this redistribution results in surface Cd atoms having no dangling bonds (i.e., approaching an sp^2-like configuration), while each surface Se atom obtains a lone pair to yield an sp^3-like configuration. The sp^2-like configuration results in a planar structure as opposed to the sp^3-like tetrahedral configuration, which is apparent in the relaxed nonpolar surfaces of Figure 3b. On the other hand, in the case of the polar facets, where Cd or Se atoms exhibit either one or three dangling bonds, there is no clear pathway for such surface relaxation.

Figure 3d shows that prior to bonding with oxygen, both polar and nonpolar facets exhibit a relatively high surface energy versus a reference state of 0 meV/Å^2 defined by eq 1 in the Supporting Information. This is due to the presence of a number of dangling bonds per surface atom (Figure 3b), which render both Cd and Se sites prone to growth. Following 100% oxygen passivation (Figure 3c), the electron deficient oxygen atoms form a strong bond with the electron-rich surface Se atoms. This lowers

© 2010 American Chemical Society

DOI: 10.1021/nl903843g | *Nano Lett.* **2010,** *10,* 680-685

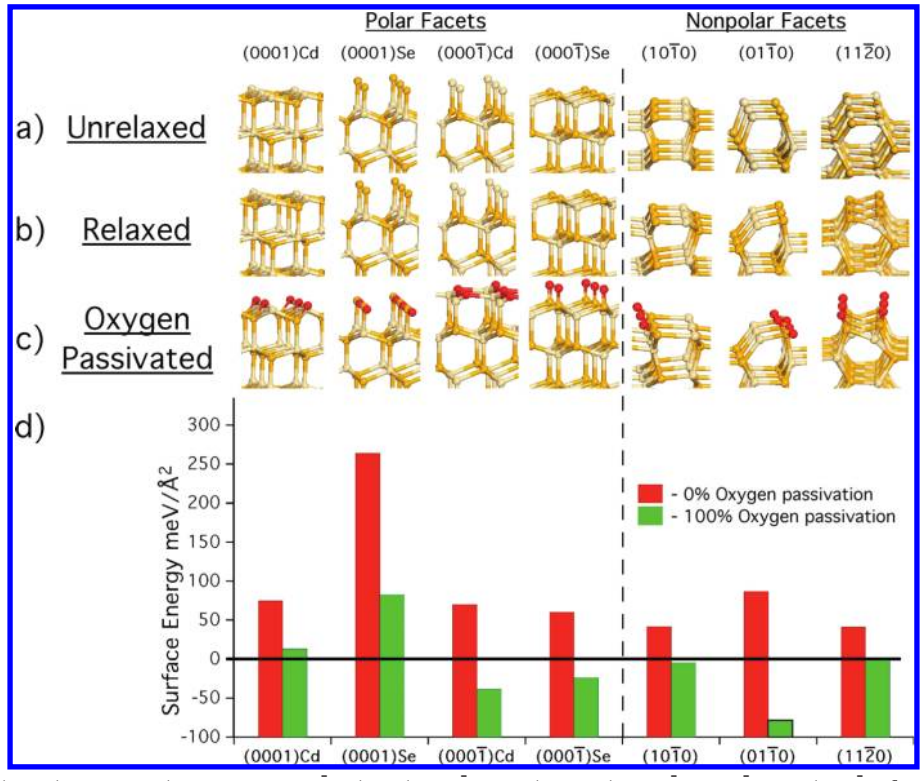

FIGURE 3. Models of the polar (0001)Cd, (0001)Se, (000$\bar{1}$)Cd, and (000$\bar{1}$)Se and nonpolar (10$\bar{1}$0), (01$\bar{1}$0), and (11$\bar{2}$0) facets in the (a) unrelaxed and (b) the relaxed states. (c) Corresponding relaxed configuration after stoichiometric binding with oxygen (red) (Cd and Se atoms are beige and orange, respectively). (d) Calculated surface energy of the facets before and after oxygen passivation.

the surface energy of all nonpolar facets to below 0 meV/Å^2 and renders these facets more resistant to growth. Here, it is important to stress that our DFT simulations indicate that, for stoichiometric facets, oxygen atoms initially prefer to interact with Se as opposed to Cd surface sites (Figure 3b).

In terms of the polar facets, the surface atom and number of dangling bonds influence the stability in the presence of oxygen. For example, the surface energy of the (000$\bar{1}$)Se facet, which has only one dangling bond per Se atom, decreases below 0 meV/ Å^2 due to the aforementioned preference of Se to bond with oxygen. However, in the case of the (0001)Se facet, the three dangling bonds per surface Se atoms present an overwhelming electron density to the oxygen atoms forcing the formation of a strong bond with one of the three dangling bonds, leaving the other two unpassivated. Since additional Se to oxygen binding is unfavorable (due to atomic crowding), the resulting surface configuration maintains a positive surface energy. In terms of oxygen binding to the Cd-terminated polar facets, the reverse situation is witnessed. Since Cd is more electron deficient than Se, a Cd atom with three dangling bonds binds the oxygen strongly at the site where the Se would have been. This renders the (000$\bar{1}$)Cd surface stable (negative surface energy) when oxygen passivated, thereby impeding NC growth from this facet. On the other hand, a Cd atom with one dangling bond does not contain sufficient electron density to strongly bind an oxygen atom, resulting in a positive energy for the (0001)Cd facet. These data corroborate the findings from Figure 2a and furthermore suggest that oxygen binding is stronger on the (000$\bar{1}$) facets as opposed to the (0001), making the latter more prone to growth. If this is a valid prediction, then the presence of oxygen makes case B in Figure 1a more preferable to case A.

To test this prediction, heterostructured nanorods were made under the same conditions as sample i by adding both $CdCl_2$ and $HgCl_2$ to a CdSe-seeded media where the size of the seed and optical density at the first absorption maximum of the seed solution are 3.5 nm and 4.0, respectively. Mercury was chosen because of the ability to spatially distinguish Hg from Cd atoms using energy dispersive X-ray analysis (EDX) in conjunction with scanning transmission electron microscopy (STEM) (see Figure S6 in Supporting Information). Such heterostructured nanorods are bound to experience significant strain based on lattice mismatch between the two components. Furthermore, HgSe has been reported to prefer the cubic zinc blende structure[23] as opposed to the wurtzite CdSe seeds. HRTEM analysis of the CdSe-seeded $Cd_xHg_{1-x}Se$ rods (Figure 4a) indicates the presence of "bent" rods with two distinct crystal structures (i.e., a short wurtzite section and a larger zinc blende region) which are joined at the "bend" in the rod. The average angle between the two sections was found to be 35° ± 3° (90% confidence) (Figure S7, Supporting Information) which co-

© 2010 American Chemical Society

DOI: 10.1021/nl903843g | *Nano Lett.* **2010,** *10,* 680-685

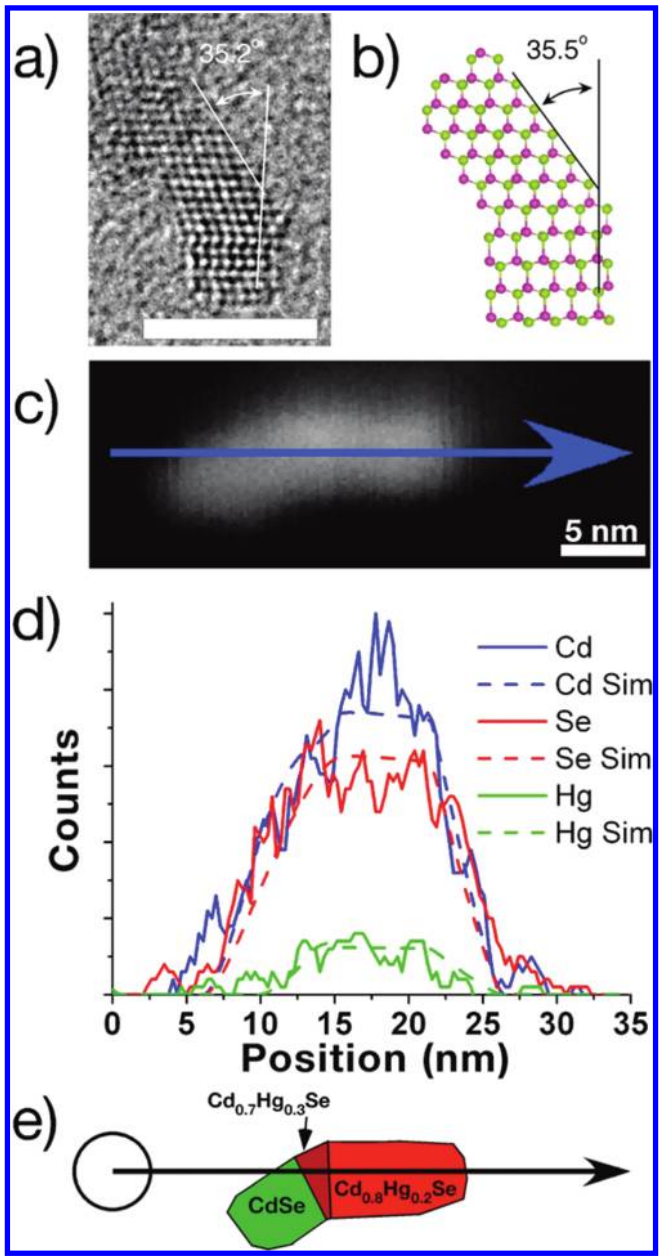

FIGURE 4. (a) Representative HRTEM image of a CdSe-seeded CdSe/$Cd_xHg_{1-x}Se$ NC. The nanocrystal appears to "bend" at the junction between zinc blende and wurtzite. The zinc blende region appears to be growing along its 001 axis. (b) Simulated image of a "bent" NC. The bend occurs at the wurtzite−zinc blende junction, and the resulting NC grows along the 001 direction in zinc blende at 35.5° from the 0001 zone axis of the wurtzite section. (c) Dark field STEM image of a CdSe−$Cd_xHg_{x-1}Se$ rod. Arrow indicates the path of the EDX line scan. (d) STEM EDX line scan of the rod in (c) overlaid with simulated line scan. The simulated scan is based on a 5 nm beam size and the rod composition shown in (e). (e) Image showing the simulation of the STEM scan. The portion in red indicates the starting CdSe QD and the green areas are $Hg_xCd_{1-x}Se$. The composition of the larger green section starts at $Cd_{0.7}Hg_{0.3}Se$ and quickly grades to $Cd_{0.8}Hg_{0.2}Se$. Simulated image is a trace of the NC in Figure 4a. Estimated beam size was 5 nm.

incides well with the simulated angle of 34.2° for a wurtzite−zinc blende CdSe junction (Figure 4b).

Figure 4c illustrates a representative CdSe-seeded $Cd_xHg_{1-x}Se$ rod imaged in dark field mode in the STEM. The path of the line scan is indicated by the blue arrow. From elemental analysis, we infer that the overall composition of the rods in the sample is $Cd_{0.76}Hg_{0.24}Se$.

Figure 4d depicts the STEM-EDX line scan of the rod in Figure 4c for Cd, Se, and Hg (see Materials and Methods in Supporting Information). While both Cd and Se are present along the entire length of the rod, Hg is observed mainly on the right side (longer arm) of the rod. Here it is important to stress that the slope of the Cd and Se traces at the beginning of the line scan is more gradual than their slope at the end of the line scan. Moreover, the signal for Hg does not begin until the bend in the NC is reached. This, in conjunction with the HRTEM results of Figure 4a, indicates that the shorter arm of the rod contains the wurtzite CdSe seed while the longer arm is zinc blende $Cd_xHg_{1-x}Se$.

In order to better understand the line-scan traces for Cd, Se, and Hg, a simulation was performed using the model in Figure 4e. The model assumes that the region of the bend closest to the CdSe seed (darker red) has a slightly higher mercury concentration than the longer arm, resulting in compositions of $Cd_{0.7}Hg_{0.3}Se$ and $Cd_{0.8}Hg_{0.2}Se$, respectively. We also assumed an effective beam size was 5.0 nm due to large positional variations in the beam from vibrations and sample drift. With this model, we were able to accurately reproduce the shape of the line-scan profiles in Figure 4b. Details of this simulation will are given in the Supporting Information section. These data support the prediction that, in the presence of oxygen, the seed growth of rods occurs not only unidimensionally but also unidirectionally, namely along [0001]. Moreover, the data of Figure 4 show that redox-assisted growth has the potential to be modified to make heterostructured NCs. More research is currently underway to explore all of the possibilities in this regard.

In conclusion, we have outlined a new synthetic means of producing QRs of high aspect ratio at low temperature (125 °C). Our results indicate that oxygen plays a key factor in directing such growth through passivation of the nonpolar facets so that growth occurs unidirectionally along the [0001] direction. We have also provided a model that shows that this is due to a reduction of the surface energy upon oxygen binding for a majority of the facets, leaving the (0001) facet alone to grow as opposed to the $(000\bar{1})$ facet. Finally we show that heterostructured rods can be seeded through this method simply by adding a different metal precursor. This seeded-growth provides a simple, low-temperature venue for producing high aspect ratio rods and heterostructures, with a number of potential applications.

Acknowledgment. The authors would like to thank Dr. Christopher Perkins for the elemental analysis results and Dr. Yong Zhang for helpful conversations. Financial Support

© 2010 American Chemical Society

DOI: 10.1021/nl903843g | *Nano Lett.* **2010,** *10,* 680-685

from NSF CBET 0828772, NSF CBET 0730365, NSF0828824, and NIH ES013557 is kindly acknowledged.

Supporting Information Available. Materials and methods section, computational details, figures showing histograms of length, width, aspect ratio, and volume for all the samples, sum EDX spectrum for CdSe-seeded/$Cd_xHg_{1-x}Se$ nanorods, and histogram of angle of bend for CdSe-seeded/$Cd_xHg_{1-x}Se$ nanorods. This material is available free of charge via the Internet at http://pubs.acs.org.

REFERENCES AND NOTES

(1) Hu, J.; Li, L.; Yang, W.; Manna, L.; Wang, L.; Alivisatos, A. P. *Science* **2001**, *292*, 2060–2063.
(2) Chen, X.; Nazzal, A.; Goorskey, D.; Xiao, M.; Peng, Z. A.; Peng, X. *Phys. Rev. B* **2001**, *64*, 245304/1–245304/4.
(3) Huynh, W. U.; Dittmer, J. J.; Alivsatos, A. P. *Science* **2002**, *295*, 2425–2427.
(4) Carbone, L.; Nobile, C.; De Giorgo>, M.; Sala, F. D.; Morello, G.; Pompa, P.; Hytch, M.; Snoeck, E.; Fiore, A.; Franchini, I. R.; Nadasan, M.; Silvestre, A. F.; Chiodo, L.; Kudera, S.; Cingolani, R.; Krahne, R.; Manna, L. *Nano Lett.* **2007**, *7* (10), 2942–2950.
(5) Talapin, D. V.; Koeppe, R.; Götzinger, S.; Kornowski, A.; Lupton, J. M.; Rogach, A. L.; Benson, O.; Feldmann, J.; Weller, H. *Nano Lett.* **2003**, *3* (12), 1677–1681.
(6) Mokari, T.; Rothenberg, E.; Popov, I.; Costi, R.; Banin, U. *Science* **2004**, *304*, 1787–1790.
(7) Sheldon, M. T.; Trudeau, P. E.; Mokari, T.; Wang, L. W.; Alivisatos, A.P.*Nano Lett.* **2009**, *9*, 3676–3682.
(8) Peng, X.; Manna, L.; Yang, W.; Wickham, J.; Scher, E.; Kadavanich, A.; Alivisatos, A. P. *Nature* **2000**, *404*, 59–61.
(9) Peng, Z. A.; Peng, X. *J. Am. Chem. Soc.* **2001**, *123*, 1389–1395.
(10) Murray, C. B.; Kagan, C. R.; Bawendi, M. G. *Science* **1995**, *270*, 1335.
(11) Tang, Z.; Kotov, N. A.; Giersig, M. *Science* **2002**, *297*, 297–240.
(12) Li, R.; Luo, Z.; Papadimitrakopoulos, F. *J. Am. Chem. Soc.* **2006**, *128*, 6280–6281.
(13) Li, R.; Lee, J.; Yang, B.; Horspool, D. N.; Aindow, M.; Papadimitrakopoulos, F. *J. Am. Chem. Soc.* **2005**, *127*, 2524–2532.
(14) Li, R.; Lee, J.; Kang, D.; Luo, Z.; Aindow, M.; Papadimitrakopoulos, F. *Adv. Funct. Mater.* **2005**, *16*, 345–350.
(15) Yu, M.; Fernando, G. W.; Li, R.; Papadimitrakopoulos, F.; Shi, N.; Ramprasad, R. *App. Phys. Lett.* **2006**, *88*, 231910.
(16) Myung, N.; Bae, Y.; Bard, A. J. *Nano Lett.* **2003**, *3* (6), 747–749.
(17) Katari, J. E. B.; Colvin, V. L.; Alivisatos, A. P. *J. Phys. Chem.* **1994**, *98*, 4109–4117.
(18) Ebina, A.; Asano, K.; Takahashi, T. *Phys. Rev. B* **1980**, *22* (4), 1980–1991.
(19) Brilson, L. J. *Surf. Sci.* **1977**, *69*, 62.
(20) Pilania, G.; Sadowski, T.; Ramprasad, R. *J. Phys. Chem. C* **2009**, *113*, 1863–1871.
(21) Séby, F.; Potin-Gautier, M.; Giffaut, E.; Borge, G.; Donard, O. F. X. *Chem. Geol.* **2001**, *171*, 173–194.
(22) Puntes, V.F.l; Krishnan, K. M.; Alivisatos, A.P.' *Science* **2001**, *291*, 2115–2117.
(23) Barnard, A. S.; Xu, H.; Li, X.; Pradhan, N.; Peng, X. *Nanotechnology* **2006**, *17*, 5707–5714.
(24) Adachi, S.; *Handbook on Physical Properties of Semiconductors*;, Springer-Verlag: Berlin, 2004; Vols. 1−3.

© 2010 American Chemical Society

DOI: 10.1021/nl903843g | *Nano Lett.* **2010,** *10,* 680-685